Title	Wireless Power Domino-Resonator Systems With Noncoaxial Axes and Circular Structures
Author(s)	Zhong, W; Lee, CK; Hui, SYR
Citation	I E E E TRANSACTIONS ON POWER ELECTRONICS, 2012, v. 27 n. 11, p. 4750-4762
Issued Date	2012
URL	http://hdl.handle.net/10722/164097
Rights	I E E E TRANSACTIONS ON POWER ELECTRONICS. Copyright © I E E E.

Wireless Power Domino-Resonator Systems With Noncoaxial Axes and Circular Structures

W. X. Zhong, Chi Kwan Lee, *Member, IEEE*, and S. Y. (Ron) Hui, *Fellow, IEEE*

***Abstract*—In this paper, a general analysis on wireless power domino-resonator systems with noncoaxial axes is presented. The mathematical formulation established can in principle be used to analyze wireless resonator systems with various domino forms. In this study, it is used to analyze and evaluate wireless domino-resonator systems with circular structures because such structures have more than one main power flow paths and have not been analyzed previously. Based on the superposition method, individual power flow paths are analyzed and then their interactions are emerged and explained with vector diagrams. Unlike the resonator pair used by Tesla, it is demonstrated that optimization of the domino systems can be achieved under "nonresonance frequency" operation and optimal load conditions. The shift of the optimal frequency from the resonance frequency is due to the multiple power flow paths. The theoretical results have been favorably verified with practical measurements obtained from two circular systems.**

***Index Terms*—Magnetic induction, wireless power transfer.**

I. Introduction

OVER a century ago, Tesla demonstrated that electric power could be transferred wirelessly through a pair of magnetically coupled coil resonators, each formed of a winding (inductor) and a capacitor. He discovered that such wireless power could be transmitted efficiently through the resonator pair at the resonant frequency of the coil resonators [1], [2]. The basic principles of 1) using *LC* resonant circuits and 2) operation at the resonant frequency laid down by Tesla for wireless power transfer through a pair of resonators are still valid today and have found many new applications in the modern era. Since 1960s, transcutaneous energy transfer for medical implants has been an active research topic [3]–[7]. In 1990s, research on wireless power transfer through human skin based on the resonant techniques to compensate the large leakage inductance of core-based coupled windings and power electronics soft-switching technology [6], [7] was reported. Such applications offer the obvious benefits of eliminating the need of surgical operations simply for replacing batteries. On the industrial front, inductive power pickup systems [8], [9] and wireless-powered lighting systems [10], in which the use of long cables is a nuisance, have been proposed. On the consumer electronics front, significant progress [11]–[16] has been made in the research, development, and commercialization of wireless charging pads for portable electronic products such as mobile phones iPods, etc. Consequently, the world's first wireless power standard "Qi" was officially launched in 2010 by the Wireless Power Consortium, which now consists of over 100 companies [17].

So far, most of these modern wireless power applications are of the "short-range" type in which the transmission distance is much smaller than the diameters of the transmitter and receiver coils. Like Tesla's previous works, they rely on the use of a pair of magnetically coupled resonators (i.e., the transmitter coil and the receiver coil), although in some cases, multiple receiver coils can be used. Due to the loosely coupled nature of the transmitter and receiver coils, capacitors are normally used to form resonant circuits in order to reduce the effects of the impedance of the leakage inductance and to enhance power flow under the operation of resonance frequency.

Tesla's wireless power idea has not found many "midrange" applications with power exceeding a few watts, although wireless power transfer of a few milliwatts has been utilized in wireless-power remote-sensor applications [18]. The reason for its not being used for relatively high power is mainly due to the deteriorating energy efficiency with the transmission distance [19], [20]. Midrange applications here refer to nonradiative wireless power transfer in which the transmission distance is larger than the diameters of the coil resonators. Fig. 1 illustrates the limitation of using a pair of resonators for wireless power transfer. The efficiency decreases exponentially with transmission distance. In order to improve the transmission efficiency, relay resonator has been proposed for power transfer [21], although such concept has been reported in waveguide and very low-power (milliwatts) wireless transmission [22]. With the use of the relay resonators, magnetically coupled resonators can be placed in closer proximity and therefore enjoy a higher energy efficiency for a given transmission distance, making such wireless power systems with more application potential for power level from several watts to a few kilowatts. If more relay resonators are used, it has been demonstrated that such wireless power resonators can be arranged in various domino forms, as shown in Fig. 2 [23]. So far, only detailed analyses of straight

Manuscript received August 8, 2011; revised October 6, 2011; accepted October 31, 2011. Date of current version June 20, 2012. This work was supported by Hong Kong Research Grant Council through project HKU-114410E. Recommended for publication by Associate Editor K. Ngo.

W. X. Zhong is with the Department of Electronic Engineering, City University of Hong Kong, Kowloon, Hong Kong (e-mail: wzhong3@student.cityu.edu.hk).

C. K. Lee is with the Department of Electrical and Electronic Engineering, The University of Hong Kong, Pokfulam, Hong Kong (e-mail: cklee@eee.hku.hk).

S. Y. R. Hui is with the Department of Electrical and Electronic Engineering, Imperial College London, London SW7 2AZ, U.K, and also with the Department of Electrical and Electronic Engineering, The University of Hong Kong, Pokfulam, Hong Kong (e-mail: ronhui@eee.hku.hk).

Color versions of one or more of the figures in this paper are available online at http://ieeexplore.ieee.org.

Digital Object Identifier 10.1109/TPEL.2011.2174655

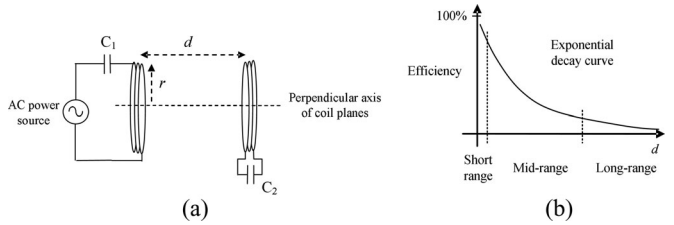

Fig. 1. (a) Wireless power transfer via a pair of coil resonators and (b) its energy efficiency variation with transmission distance.

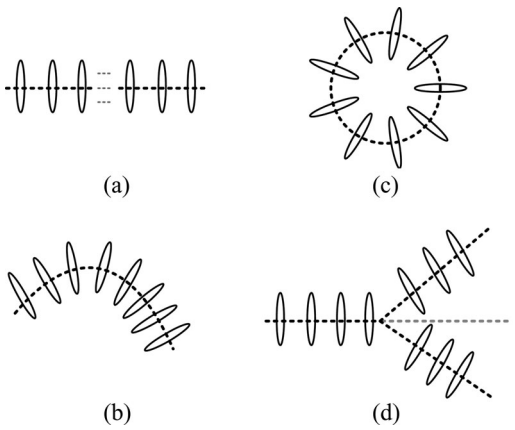

Fig. 2. Various domino forms of wireless power resonators [23].

wireless domino-resonator systems have been reported. Straight domino-resonator systems have the unique features that their centers of the resonators lie along the same axis and there is only one main power flow path. Our literature search has revealed that no detailed analysis has been reported about the behavior of wireless domino-resonator systems with noncoaxial axes. In particular, there will be two main power flow paths if the resonators are arranged in a circular structure because power can flow in both the clockwise and anticlockwise directions.

In this paper, the general mathematical formulation suitable for analyzing wireless domino-resonator systems with noncoaxial axes is first presented. Then such method is applied to studying the circular domino structures. Based on the superposition method, each power path is first investigated before all the paths are combined together so as to study their overall effects under resonance frequency operations. The current components in each resonator arising from each power flow path and their interactions will be explained with the aid of vector diagrams, which provide the physical insights into the combined effects of the power flow paths and allow system designers to predict their behavior. Afterwards, the investigation is extended to cover the situations in which the operating frequency deviates from the resonance frequency and in which the frequency, compensating capacitor, and load are optimized. It will be shown that the optimal frequency will deviate from the resonance frequency when there is more than one power flow path. The analytical results have been favorably confirmed with practical measurements obtained from two circular domino systems.

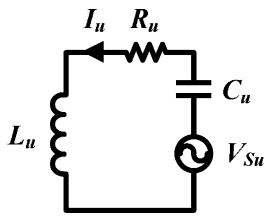

Fig. 3. Circuit model of resonator *u* in a domino-resonator system.

II. Modeling of Wireless Domino-Resonator Systems With Noncoaxial Axes

Domino-resonator systems can be implemented in many different forms, as shown in Fig. 2. However, all the systems regardless of their forms can be expressed with the coupled circuit equations that have been well developed for electric machine theory, as shown in (1), at the bottom of this page, where, as shown in Fig. 3, R_u is the resistance, X_u is the impedance $\omega L_u - 1/(\omega C_u)$, L_u is the inductance, C_u is the capacitance, I_u is the current, and V_{Su} is the voltage source in resonator *u* (i.e., the *u*th resonator in the system with *n* resonators), respectively; M_{ij} is the mutual inductance between resonator *i* and resonator *j*; ω is the angular frequency. For the loaded resonator (say the *m*th resonator), R_m ($m = 1,2,\ldots,n$) includes both the winding resistance and the load resistance.

For optimization and comparison purposes, the energy efficiency (η) is used as the indicator for system performance. It is defined as follows:

$$\eta = \frac{I_x^2 R_L}{I_1^2 R_1 + I_2^2 R_2 + \cdots + I_n^2 R_n} \tag{2}$$

where R_L is the load resistance; resonator *x* is loaded, and R_x includes both the parasitic resistance of resonator *x* and the load R_L.

A. Mutual Inductance for Coaxial Resonators

For two coaxial circular filamentary current loops, Maxwell [24] has derived a well-known equation to calculate the mutual inductance

$$M = \mu_0 \frac{\sqrt{r_1 r_2}}{\alpha}[(2-\alpha^2)K(\alpha) - 2E(\alpha)] \tag{3}$$

$$\begin{bmatrix} R_1 + jX_1 & j\omega M_{12} & j\omega M_{13} & \cdots & \cdots & j\omega M_{1n} \\ j\omega M_{12} & R_2 + jX_2 & j\omega M_{23} & \cdots & \cdots & j\omega M_{2n} \\ \vdots & \vdots & \ddots & \vdots & \vdots & \vdots \\ j\omega M_{1(n-1)} & \cdots & \cdots & \cdots & R_{n-1} + jX_{n-1} & j\omega M_{(n-1)n} \\ j\omega M_{1n} & \cdots & \cdots & \cdots & j\omega M_{(n-1)n} & R_n + jX_n \end{bmatrix} \cdot \begin{bmatrix} \mathbf{I_1} \\ \mathbf{I_2} \\ \vdots \\ \mathbf{I_{n-1}} \\ \mathbf{I_n} \end{bmatrix} = \begin{bmatrix} \mathbf{V_{S1}} \\ \mathbf{V_{S2}} \\ \vdots \\ \mathbf{V_{S(n-1)}} \\ \mathbf{V_{Sn}} \end{bmatrix} \tag{1}$$

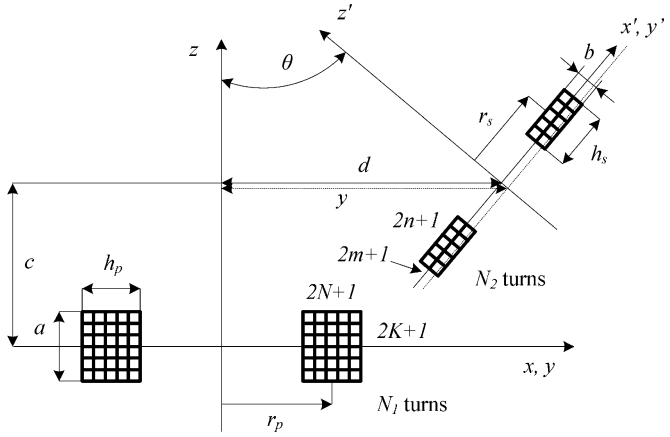

Fig. 4. Diagram of two noncoaxial circular coils [26].

where $K(\alpha)$ and $E(\alpha)$ are complete elliptic integrals of the first and second kind, respectively, and

$$\alpha = \sqrt{\frac{4r_1 r_2}{d^2 + (r_1 + r_2)^2}} \tag{4}$$

where r_1, r_2, and d are the radii of loop 1, loop 2, and the distance between them, respectively.

For two coaxial circular windings, if the wire is relatively thin comparing to the dimension of the windings so that each turn of the windings can be considered as a filamentary current loop, then the mutual inductance between the two windings can be worked out by the following:

$$M = \sum_{i=1}^{n_1} \sum_{j=1}^{n_2} M_{ij} \tag{5}$$

where n_1 and n_2 are the numbers of turns of the two windings, respectively; M_{ij} is the mutual inductance between the ith turn of the first winding and the jth turn of the second winding, which can be obtained with (3).

B. Mutual Inductance for Noncoaxial Resonators

Based on the calculation method for the mutual inductance between two filamentary circular current loops with inclined axes in [25], a mutual inductance equation for noncoaxial coils is proposed in [26] (see Fig. 4) as follows:

$$M = \frac{N_1 N_2 \sum_{g=-K}^{K} \sum_{h=-N}^{N} \sum_{l=-n}^{n} \sum_{p=-m}^{m} M(g,h,l,p)}{(2K+1)(2N+1)(2n+1)(2m+1)} \tag{6}$$

where

$$M(g,h,l,p) = \frac{\mu_0}{\pi} \sqrt{r_p(h) r_s(l)} \int_0^{\pi} \times \frac{(\cos\theta - (y(p)/r_s(l))\cos\phi)\Psi(k)}{V^{3/2}} d\phi$$

$$V = \sqrt{1 - \cos^2\phi \sin^2\theta - 2\frac{y(p)}{r_s}\cos\phi\cos\theta + \frac{y^2(p)}{r_s^2}}$$

$$\Psi(k) = \left(\frac{2}{k} - k\right) K(k) - \frac{2}{k} E(k) = \mathrm{Q}_{1/2}(x), x = \frac{2-k^2}{k^2}$$

$$y(p) = d + \frac{b\sin\theta}{2m+1} p, \qquad p = -m, ..., 0, ..., m$$

$$r_p(h) = r_p + \frac{h_p}{2N+1} h, \qquad h = -N, ..., 0, ..., N$$

$$r_s(l) = r_s + \frac{h_s}{2n+1} l, \qquad l = -n, ..., 0, ..., n$$

$$z(g,p) = c + \frac{a}{2K+1} g - \frac{b\cos\theta}{2m+1} p, \qquad g = -K, ..., 0, ..., K$$

$$p = -m, ..., 0, ..., m$$

$$k^2 = \frac{4\gamma V}{(1+\gamma V)^2 + \xi^2}, \qquad \xi = \beta - \gamma\cos\phi\sin\theta$$

$$\gamma = \frac{r_s(l)}{r_p(h)}, \qquad \beta = \frac{z(g,p)}{r_p(h)}$$

N_1 is number of turns of the larger coil; N_2 is the number of turns of the smaller coil; r_P is the radius of the larger coil; h_p is the thickness of the larger coil; a is the axial length of the larger coil; r_s is the radius of the smaller coil; h_s is the thickness of the smaller coil; b is the axial length of the smaller coil; c is the distance between coils' centers; d is the distance between coil planes; θ is the angle between axes; $K(k)$ is the complete elliptic integral of the first kind; $E(k)$ is the complete elliptic integral of the second kind; $Q_{1/2}(k)$ is the Legendre function of the second kind and half-integral degree.

Based on (6), the mutual inductances of a circular domino-resonator system, as shown in Fig. 2(c), can be determined in order to evaluate and optimize the performance of the system with the help of the general circuit (1).

III. Analysis on Circular Domino-Resonator Systems

A. Magnetically Coupled Model of the Circular Domino-Resonator System

With the use of the general magnetically coupled circuit (1) and the mutual inductance (5), wireless domino-resonator systems with noncoaxial resonators can now be analyzed. Fig. 5 shows the configuration of a circular domino-resonator system with n identical circular resonators in which all the centers of the resonators are placed on a circular path with radius r_{path} and the center of each resonator is placed in a same plane with the center of the circular path. Other parameters in Fig. 5 are: r_w is the radius of the windings; θ_1 to θ_n are the angles between every two adjacent resonators. For a given set of circuit parameters of the resonators (see Fig. 3), the number of the resonators (n), and the load resistance, the circular domino-resonator system can be defined by the radius of the circular path (r_{path}) and the angles between every two adjacent resonators (θ_1 to θ_n) with the help of (5).

A practical example of the wireless domino-resonator system under investigation is shown in Fig. 6 in which eight resonators are placed in a circular domino form, with resonator 1 excited by an ac power source and resonator 5 loaded with a compact

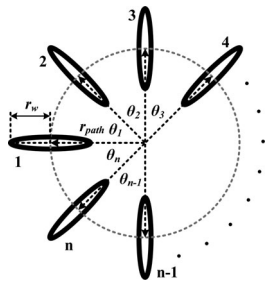

Fig. 5. Configuration of a circular domino-resonator system with ***n*** identical circular resonators.

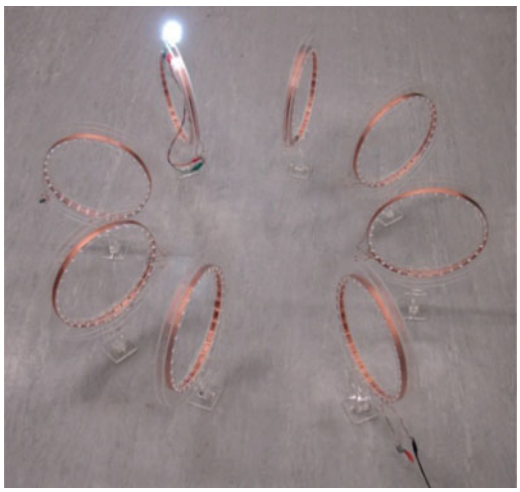

Fig. 6. Practical example of a circular wireless domino-resonator system powering a 14 W compact fluorescent lamp.

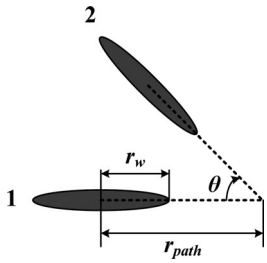

Fig. 7. Two resonators placed in a circular curve.

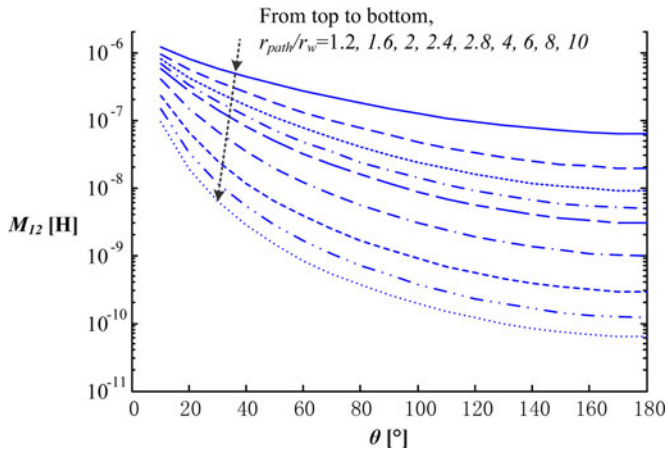

Fig. 8. Variation of the mutual inductance of two filamentary current loops with angular displacement for a set of r_{path}/r_w ratios.

fluorescent lamp of 14 W. These resonators are used in several circular forms in this study. The parameters of each resonator are listed in Table II.

In order to get some physical insights into the mutual coupling between two resonators placed along the circular path, two resonators, as shown in Fig. 7, are used to illustrate the variation of the mutual inductance as functions of the ratio of the radius of the circular path and the radius of the coil forming the resonator with the angular displacement. Fig. 8 shows the variations of the mutual inductance of two filamentary current loops (r_w of 0.5 m) with the angular displacement (θ) for a range of radii of the circular path (r_{path}). Some of the results of Fig. 8 are listed in Table I. It is noted that the mutual inductance decreases rapidly with increasing θ, which agrees with our intuitive understanding that the coupling between two coils will be worst when θ increases for a given r_{path} due to the increasing arc of magnetic flux between the centers of the coils.

B. Simplified Analysis of Circular Domino-Resonator Systems at Resonance Frequency and Optimized Load Without Considering Couplings of Nonadjacent Resonators

1) Assumptions: In this section, a simplified analysis on the circular domino-resonator systems is carried out with the following assumptions.

1) In the general circular system of Fig. 5, resonator 1 is excited by an ac power source and only resonator 2 to resonator *n* could be loaded.
2) The resonators with parameters defined in Table II are used. All resonators are evenly placed in the circular path in each setup and test, which means that the angular displacements are the same ($\theta_1 = \cdots = \theta_n$).
3) All the mutual inductances between two adjacent windings are the same (2.647 μH) in all the tested systems in order to compare the performance between the different systems with different numbers of resonator. This means that the radius of the circular path will be changed accordingly when the total number of the resonators in the system is changed.
4) Resonator 1 is excited by the ac power source at the "resonance frequency" of the resonators described in Table II.
5) Couplings between nonadjacent resonators are not considered at this stage.

2) Energy Efficiency of Circular Domino-Resonator Systems With One Load Resistor Connected to Each Resonator: For a circular domino-resonator system with all the parameters given (except the load), the efficiencies of the systems will reach the peak when the value of the load resistance R_L is optimized. Based on the use of (1), (2), (6), and the MATLAB optimization tool, the maximum energy efficiencies of a range of domino-resonator systems with the number of resonators from 3 to 10 have been computed under the assumptions listed previously.

TABLE I
MUTUAL INDUCTANCES OF TWO FILAMENTARY CURRENT LOOPS [H]

r_{path}/r_w / θ/°	1.2	1.6	2	2.4	2.8	4	6	8	10
15	9.63E-07	7.17E-07	5.70E-07	4.66E-07	3.88E-07	2.37E-07	1.18E-07	6.48E-08	3.87E-08
30	5.78E-07	3.69E-07	2.58E-07	1.88E-07	1.41E-07	6.68E-08	2.50E-08	1.16E-08	6.25E-09
45	3.85E-07	2.14E-07	1.34E-07	8.99E-08	6.28E-08	2.57E-08	8.52E-09	3.75E-09	1.96E-09
60	2.71E-07	1.33E-07	7.67E-08	4.83E-08	3.22E-08	1.21E-08	3.81E-09	1.64E-09	8.48E-10
75	1.98E-07	8.70E-08	4.72E-08	2.85E-08	1.84E-08	6.62E-09	2.02E-09	8.59E-10	4.42E-10
90	1.49E-07	6.00E-08	3.10E-08	1.81E-08	1.15E-08	4.02E-09	1.20E-09	5.09E-10	2.61E-10
105	1.17E-07	4.34E-08	2.16E-08	1.24E-08	7.76E-09	2.65E-09	7.84E-10	3.31E-10	1.69E-10
120	9.44E-08	3.30E-08	1.60E-08	9.01E-09	5.59E-09	1.88E-09	5.53E-10	2.33E-10	1.19E-10
135	7.95E-08	2.64E-08	1.25E-08	6.98E-09	4.31E-09	1.44E-09	4.20E-10	1.76E-10	9.00E-11
150	6.99E-08	2.24E-08	1.05E-08	5.79E-09	3.55E-09	1.18E-09	3.43E-10	1.44E-10	7.34E-11
165	6.46E-08	2.02E-08	9.36E-09	5.15E-09	3.15E-09	1.04E-09	3.03E-10	1.27E-10	6.47E-11
180	6.29E-08	1.95E-08	9.01E-09	4.95E-09	3.03E-09	9.99E-10	2.90E-10	1.22E-10	6.20E-11

TABLE II
PARAMETERS OF THE PRACTICAL RESONATORS

Radii of the winding	155mm	Layers of the wire	1
Number of turns	11	Axial Length of the winding	15mm
Structure of the wire	Ø0.12mm×50strands Outer Ø1.2mm	Inductance	90.7μH
Capacitance	1.036nF (Sum of the external capacitor 1.019nF and the parasitic capacitance of the winding 0.017nF)	Resistance (at 520kHz)	0.92Ω

TABLE III
MAXIMUM EFFICIENCY OF THE RESONATOR SYSTEMS UNDER DIFFERENT LOADED POSITIONS

Maximum Efficiency [%] (the sequence numbers of the loaded resonators)							
3-resonator	4-resonator	5-resonator	6-resonator	7-resonator	8-resonator	9-resonator	10-resonator
70.68 (2, 3)	**0.07** **(2, 4)**	55.40 (2, 5)	72.78 (2, 6)	44.73 (2, 7)	**0.61** **(2, 8)**	37.79 (2, 9)	59.40 (2, 10)
	80.82 (3)	63.61 (3, 4)	**2.92** **(3, 5)**	58.55 (3, 6)	69.20 (3, 7)	54.71 (3, 8)	**10.90** **(3, 9)**
			72.65 (4)	49.10 (4, 5)	**0.07** **(4, 6)**	39.64 (4, 7)	58.89 (4, 8)
					65.31 (5)	44.39 (5, 6)	**1.00** **(5, 7)**
							58.72 (6)

The results are listed in Table III. For the five-resonator system in the third column of Table III, for example, the load is connected to resonator 2 first and then to resonator 3. Because of the symmetry of the evenly spaced circular systems (see Fig. 5), the five-resonator system loaded at resonator 2 (or resonator 3) is the same as that loaded at resonator 5 (or resonator 4).

Close examination on the computed maximum energy efficiencies of this range of domino-resonator systems leads to the following four important observations.

1) When n is odd, the maximum energy efficiencies fall within a reasonably close range in all loaded resonators and there does not exist near-zero efficiency in the system.
2) When n is even, there exist very low maximum energy efficiencies when the load is connected to certain resonators. These figures are highlighted in bold type in Table III. For example, for the four-resonator system in column 2, the maximum energy efficiency is only 0.07% when the load is connected to resonator 2 or resonator 4. For the eight-resonator system in column 6, the maximum efficiencies

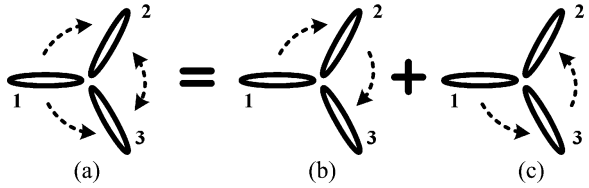

Fig. 9. Two power paths in the circular domino-resonator system.

are close to zero when the load is connected to resonator 2, 4, 6, or 8.

3) When n is even, it can be expressed as $n = 2k$. When k is even (e.g., $n = 4 = 2 \times 2$ and $n = 8 = 2 \times 4$), the maximum efficiency is very low when the even-numbered resonators are loaded and high when odd-numbered resonators are loaded. On the contrary, when k is odd (e.g., $n = 6 = 2 \times 3$ and $n = 10 = 2 \times 5$), the efficiency is low when the odd-numbered resonators are loaded and high when even-numbered resonators are loaded.
4) Comparison of the systems with odd and even n shows that, while the systems with even number of resonators have some loaded conditions with very low maximum efficiency, they do offer higher maximum efficiency than the odd-numbered counterpart if the appropriate resonators are loaded. For examples, for the four-resonator system loaded at resonator 3, the six-resonator system loaded at resonator 2 (or 4, 6), and the eight-resonator system loaded at resonator 3 (or 7), the maximum efficiencies are close to or higher than 70%, while the highest efficiency within all the systems with odd number of resonators is only 70.68% (in the three-resonator system).

3) Physical Explanation Based on Superposition Analysis and Vector Diagrams: The four important observations made previously can be analyzed with the coupled circuit model (1) and the superposition principle. One interesting feature of the circular domino-resonator systems is that resonator 1 excited by the ac power source will transfer power in both the clockwise and anticlockwise directions. Starting with the three-resonator system as an example, Fig. 9 shows the two power flow paths, with one being clockwise [see Fig. 9(b)] and the other anticlockwise [see Fig. 9(c)]. For a given input ac current $\mathbf{I_1}$, the current vectors in other resonators in the three-resonator system can be determined with following equations:

$$j\omega M_{12}\mathbf{I_1} + R_2\mathbf{I_2} + j\omega M_{23}\mathbf{I_3} = 0 \tag{7}$$

$$j\omega M_{13}\mathbf{I_1} + j\omega M_{23}\mathbf{I_2} + R_3\mathbf{I_3} = 0. \tag{8}$$

By applying the superposition principle, the coupled circuit equations for the clockwise path 1 in Fig. 9(b) when $M_{13} = 0$ become

$$j\omega M_{12}\mathbf{I_1} + R_2\mathbf{I_{2\_P1}} + j\omega M_{23}\mathbf{I_{3\_P1}} = 0 \tag{9}$$

$$j\omega M_{23}\mathbf{I_{2\_P1}} + R_3\mathbf{I_{3\_P1}} = 0. \tag{10}$$

Similarly, the corresponding equations for the anticlockwise path 2 in Fig. 9(c) when $M_{12} = 0$ are as follows:

$$R_2\mathbf{I_{2\_P2}} + j\omega M_{23}\mathbf{I_{3\_P2}} = 0 \tag{11}$$

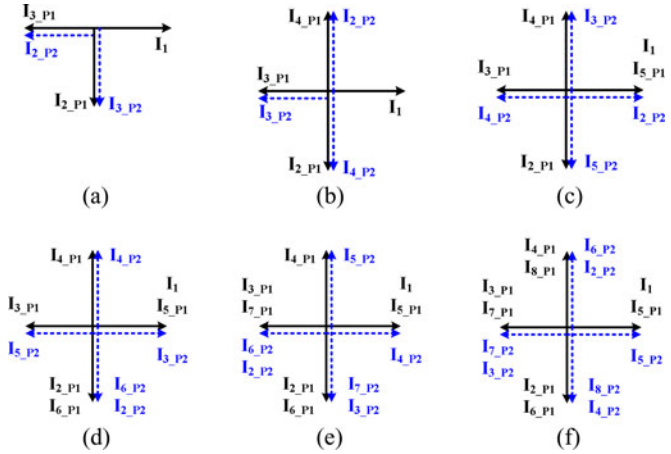

Fig. 10. Vector diagrams of the current vectors for domino-resonator system with $n = 3$ to 8 (magnitude not to scale). (a) $n = 3$. (b) $n = 4$. (c) $n = 5$. (d) $n = 6$. (e) $n = 7$. (f) $n = 8$.

$$j\omega M_{13}\mathbf{I_1} + j\omega M_{23}\mathbf{I_{2\_P2}} + R_3\mathbf{I_{3\_P2}} = 0 \tag{12}$$

where $\mathbf{I_{2\_P1}}$ and $\mathbf{I_{3\_P1}}$ represent the currents induced in resonator 2 and resonator 3 in path 1 [see Fig. 9(b)]; $\mathbf{I_{2\_P2}}$ and $\mathbf{I_{3\_P2}}$ represent the currents induced in the corresponding resonators in path 2 [see Fig. 9(c)]. The resultant current vectors for $\mathbf{I_2}$ and $\mathbf{I_3}$ in the three-resonator system are therefore as follows:

$$\mathbf{I_2} = \mathbf{I_{2\_P1}} + \mathbf{I_{2\_P2}} \tag{13}$$

$$\mathbf{I_3} = \mathbf{I_{3\_P1}} + \mathbf{I_{3\_P2}}. \tag{14}$$

From (10), we can easily get

$$\mathbf{I_{3\_P1}} = \frac{-j\omega M_{23}}{R_3}\mathbf{I_{2\_P1}} \tag{15}$$

which shows that $\mathbf{I_{3\_P1}}$ should lag behind $\mathbf{I_{2\_P1}}$ by 90°. By substituting (15) into (11), we get

$$\mathbf{I_{2\_P1}} = \frac{-j\omega M_{12}}{R_2 + \omega^2 M_{23}^2/R_3}\mathbf{I_1} \tag{16}$$

which implies that the reflected impedance of the resonator 3 on resonator 2 is resistive ($\omega^2 M_{23}^2/R_3$) resulting $\mathbf{I_{2\_P1}}$ lags behind $\mathbf{I_1}$ by 90°. Similarly, for path 2, $\mathbf{I_{2\_P2}}$ lags behind $\mathbf{I_{3\_P2}}$ by 90° and $\mathbf{I_{3\_P2}}$ lags behind $\mathbf{I_1}$ by 90°. The analysis can be easily extended to an n-resonator system and the results can be summarized into one simple rule that the induced current lags behind the source current by 90°. For example, in a eight-resonator system, $\mathbf{I_{7\_P1}}$ is the induced current of $\mathbf{I_{6\_P1}}$, which implies that $\mathbf{I_{6\_P1}}$ is the source current for $\mathbf{I_{7\_P1}}$ and $\mathbf{I_{7\_P1}}$ should lag behind $\mathbf{I_{6\_P1}}$ by 90°; while in path 2 (anticlockwise), $\mathbf{I_{7\_P2}}$ is the source current for $\mathbf{I_{6\_P2}}$ resulting that $\mathbf{I_{6\_P2}}$ lags behind $\mathbf{I_{7\_P2}}$ by 90°.

The results tabulated in Table III can then be explained with the help of the vector diagrams showing the phase relationships of the currents. Based on the above analysis, the vector diagrams (not to scale) for the resonator systems with $n = 3$ to 8 are given in Fig. 10(a)–(f), respectively. These vector diagrams provide the physical insights into the behavior of these circular domino-resonator systems.

Careful inspections of the vector diagrams in Fig. 10 can offer the explanations to the following four observations.

1) The vector diagrams of the systems with odd number of resonators in Fig. 10(a), (c), and (e) for $n = 3$, 5, and 7, respectively, indicate that that the two current vectors due to the two power flow paths in each resonators are always perpendicular (i.e., $\mathbf{I_{x\_P1}}$ and $\mathbf{I_{x\_P2}}$ have a phase shift of 90° for each resonator $\mathbf{x}$). This means that these two currents in each resonator neither counteract each other nor fully reenforce each other. This is the reason for observation 1 that their maximum efficiencies fall fairly close to each other, but they do not have high maximum efficiency as the systems with even number of resonators enjoy, as will be discussed.
2) The vector diagram of Fig. 10(b) for the four-resonator system shows that the two current vectors due to the two paths in Resonator 3 are in phase, i.e., $\mathbf{I_{3\_P1}}$ and $\mathbf{I_{3\_P2}}$ are in phase and thus fully reenforcing each other. However, the current vector pairs $\mathbf{I_{2\_P1}}$ and $\mathbf{I_{2\_P2}}$ are out of phase and thus counteracting each other, and so do $\mathbf{I_{4\_P1}}$ and $\mathbf{I_{4\_P2}}$. This explains why the maximum efficiency of the four-resonator system is close to zero (0.07%) when either resonator 2 or resonator 4 is loaded, and the maximum efficiency is high (80%) when resonator 3 is loaded. The current vector counteraction in systems with even number of resonators gives the explanation to observation 2. Similar arguments can apply to other systems with even number of resonators. It should be noted that the vectors in Fig. 10 show only the phase relationships of the currents (i.e., the magnitude is not to scale), the counteraction of two currents does not result in a zero current (i.e., zero output power). Consequently, a very low overall efficiency is recorded.
3) While the current vector pairs in the odd-numbered resonators (resonators 3 and 5) are out of phase and they counteract each other in the six-resonator system [see Fig. 10(d)] in which $n = 6 = 2 \times 3$ indicates that $k = 3$ is an odd number, the vector diagram of the eight-resonator system ($k = 4$) in Fig. 10(f) shows that the current pairs in the even-numbered resonators (resonators 2, 4, 6, and 8) are out of phase, and the current pairs in the odd-numbered resonators (resonators 3, 5, and 7) are in phase. This physical insight is consistent with the observation 3.
4) The fact that certain current pairs in the systems with even number of resonators can be in phase and fully reenforce each other gives an explanation to why they enjoy higher maximum efficiency than systems with odd number of resonators, which have their current pairs always 90° out of phase in each resonator. This feature is consistent with observation 4.

C. Analysis of the Multiple Power-Path Effects of the Circular Three-Resonator System With Optimized Load and Operating Frequency

1) Effects Of Multiple Power Paths and the Operating Frequency on the Optimal Operation of the Domino-Resonator Systems: While the simplified analysis in the previous subsection enables one to understand the interactions of the two power flow paths, it is necessary in many cases to include the couplings among the nonadjacent resonators in the analysis in order to determine the optimal energy efficiency operating point more precisely. It should be noted that the principle of optimal operation at the resonance frequency for wireless power transfer proposed by Tesla is only valid for a pair of resonators. It has been proved that the couplings among nonadjacent resonators will provide more than one power path, which could shift the optimal frequency slightly away from the resonance frequency in a straight domino-resonator system [23]. In the circular domino-resonator systems studied here, there will be at least two power paths even if the couplings between the nonadjacent resonators are neglected. Therefore, the optimal frequency will also be expected to shift away from the resonance frequency.

The analysis in the previous subsection is based on the system operating at resonance frequency of the resonators and with the load optimized only. When both of the operating frequency and the load can become variables for maximizing the energy efficiency, the efficiency of the circular-resonator systems can be further improved. In the following analysis, the winding resistance of the resonators is assumed to be constant because of the small range of frequency variation. The radius of the circular path r_{path} is 300 mm. Both (6) and the Maxwell finite-element analysis (FEA) software are used to work out the mutual inductance between two resonators. The results from the two methods are consistent and are rounded to 2.647 μH. The 3-D plot of the energy efficiency of the three-resonator system with the operating frequency and load is displayed in Fig. 11, where f_0 represents the resonance frequency of the resonators (which is 519.2 kHz). The highest efficiency occurs at the operating point at which the load is 17.78 Ω, the ratio of f/f_o is 0.985 and the energy efficiency is 80.97%. This is not the exact optimum point because the 3-D plot is generated by scanning the variables with certain step length. The exact optimum point can be found out as (R_L, f/f_0, η) = (17.04 Ω, 0.9855, 81.00%) with the help of MATLAB optimization toolbox. For the plane of $R_L = 17.04\ \Omega$, the variation of the energy efficiency with f/f_o is plotted in Fig. 12. It can be seen that the energy efficiency at f_o is 70.52%, while that at 0.9855 f_o is 81%, resulting in an improvement of over 10%. The optimum frequency range is found out to be from $0.9766f_0$ to $0.9929f_0$ (507.05–515.51 kHz) in which the degradation of the efficiency is kept within 2% from the maximum value (at $0.9855f_0$). Beyond $0.9929f_0$, the efficiency decreases fast. Therefore, the optimum operating frequency of the domino-resonator system with more than two resonators is not necessarily the natural resonance frequency of the resonators.

2) Altering the Power Flow by Adjusting Resonator Impedance for Maximizing Efficiency in Targeted Resonator Under a Given Operating Frequency: Besides varying the operating frequency, it is also possible to alter the resonator impedance in order to change the impedance of the power flow paths and direct the power to a targeted resonator.

First of all, the operating frequency should be decided. In a two-resonator system, it has been proven that higher

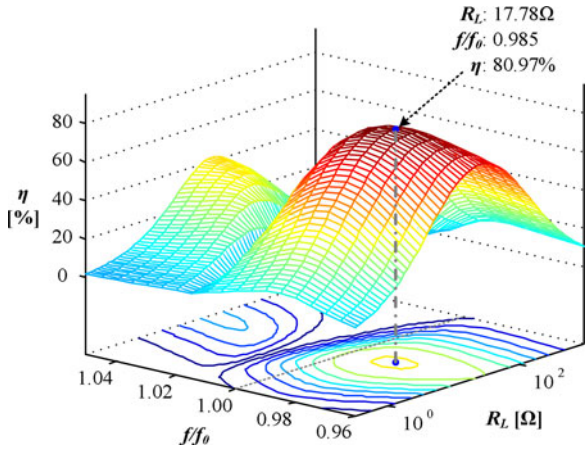

Fig. 11. 3-D plot of the energy efficiency of the circular three-resonator system as a function as f/f_0 and R_L.

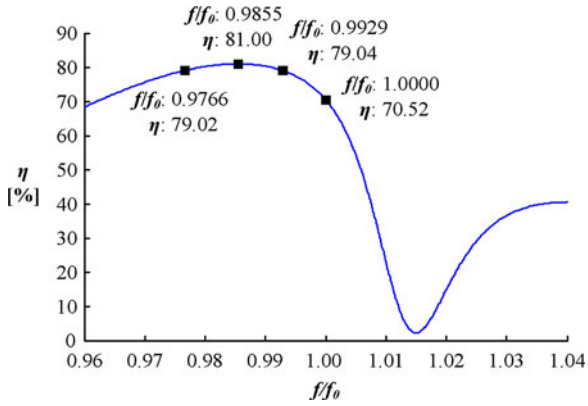

Fig. 12. Energy efficiency of the circular three-resonator system as a function as f/f_0 when R_L is 17.04 Ω.

Q factors [$Q = \omega L/R$] of the coils lead to higher power transfer efficiency [20]. Therefore, it is reasonable to conclude that higher Q factors of the coils will also lead to higher efficiency in a system with more than two resonators provided that other variables of the system are optimized so that each resonator in the system offers positive contribution to the overall performance, which is correct in the case of the circular resonator systems. Therefore, for given identical windings, an impedance analyzer can be used to find out the optimum frequency at which the quality factor of the windings peaks. In this study, the windings used for the resonators (see Table II) have the highest Q factor at about 520 kHz. For a winding with self-inductance of 90.7 μH, a compensating capacitor of 1 nF (or practically 1.036 nF including parasitic capacitance of the windings) will give a natural resonance frequency of about 519.2 kHz. Since changing this external capacitance is easier than changing the number of turns (and inductance) of the coils, altering the compensating capacitance is an obvious choice to change the impedance of the resonators.

With the help of a MATLAB optimization toolbox, an exercise to maximize the energy efficiency in a three-resonator system has been conducted to vary the compensating capacitors when resonator 3 is loaded and the operating frequency is set at

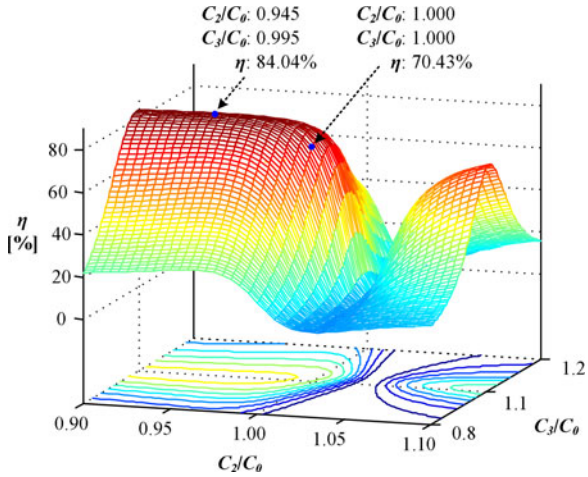

Fig. 13. 3-D plot of the efficiency of the circular three-resonator system as a function as C_2/C_0 and C_3/C_0.

519.2 kHz. A maximum energy efficiency of 84.05% occurs at the optimized conditions of $C_2 = 0.9448C_0$, $C_3 = 0.9942C_0$, and $R_L = 12.72\ \Omega$. The 3-D plot of the energy efficiency is plotted in Fig. 13 for $R_L = 12.72\ \Omega$.

It is noted that the optimized C_3 is almost identical to C_0. In practice, capacitors have discrete values. The capacitance value next to 1 nF is 910 pF. If one chooses $C_3 = C_0$ and $C_2 = 0.91C_0$, the test conditions with (1) only R_L optimized, (2) both the frequency f and R_L optimized, and (3) C_2, C_3, and R_L optimized, the results are computed and tabulated in Table IV. It can be seen that over 10% improvement in energy efficiency can be achieved by the last two methods for the three-resonator system.

Strictly speaking, further optimization can be achieved if f, C_2, C_3, and R_L are all considered as variables simultaneously. In this case, the ac resistance of the windings is frequency dependent and can no longer be considered as a constant as in case (2) where the frequency is within a narrow range. The expression will therefore be more complicated and is beyond the scope of this paper.

D. Optimum Operations of the Circular Four-Resonator System

The performance of a circular four-resonator system (see Fig. 14) is also investigated. The mutual inductance between two adjacent resonators of the four-resonator system is also 2.647 μH with the radius of the circular path r_{path} of 235 mm. In this case, the mutual inductances between resonator 1, 3 and 2, 4, (i.e., M_{13} and M_{24}) are 0.8939 μH according to the FEA result and (6). Since M_{13} and M_{24} are about 0.34 times the M_{12} (M_{23}, M_{34}, and M_{41}), they are included in the full system model (1) for this investigation. Tables V and VI show the calculated results for the four-resonator system with resonators 2 and 3 loaded, respectively.

The results tabulated in Table V point to one very important point about the limitation of having low energy efficiency (due to current vector counteraction, as illustrated in Fig. 10) in certain resonators in the systems with even number of resonators under

TABLE IV
EFFICIENCY COMPARISON UNDER PRACTICAL CONSIDERATION FOR THE CAPACITORS

	C_2/C_0	C_3/C_0	f/f_0	$R_L[\Omega]$	η
OPT(R_L)	1	1	1	14.98	70.68%
OPT(f, R_L)	1	1	0.9855	17.05	81.00%
OPT(C_2, C_3, R_L)	0.9	1	1	11.03	83.42%

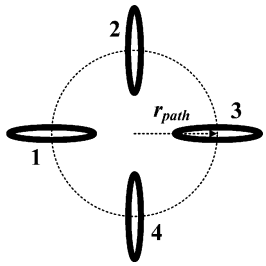

Fig. 14. Circular four-resonator system.

the resonance frequency operation. For a four-resonator system, Table III shows that the efficiency of the system under resonance operation is close to zero if either resonator 2 or 4 is loaded. The results in Table V indicates that such limitation can be eliminated either by deviating the operating frequency from the resonance frequency or by altering the impedance of the resonators (via changes in capacitor values). This phenomenon is different from Tesla's experiment on the use of one pair of resonators. The theoretical results show that an energy efficiency of 75% to 83% can be achieved via the optimization of the frequency and the load, or the capacitor values and the load. When the load is connected to resonator 3, the theoretical results are included in Table VI. Again, over 80% of energy efficiency can be achieved by nonresonance frequency operation.

IV. EXPERIMENTAL VERIFICATION

Experiments have been carried out with a circular three-resonator and a circular four-resonator system (see Fig. 15) in order to verify the theoretical analysis. While Fig. 6 shows that such circular domino-resonator system can power a 14 W lamp, resistive loads are used in this experimental verification, particularly when the load has to be optimized. The radii of the circular paths (r_{path}) of the three-resonator and four-resonator systems are designed to be 300 and 235 mm, respectively, which keep the mutual inductances between adjacent windings of the two systems the same. Resonator 1 is driven by an RF power amplifier with magnitude and frequency control. The currents in each resonator are recorded by a digital storage oscilloscope so that their vector diagrams can be produced.

A. Circular Three-Resonator System

A circular three-resonator system is used for the three practical tests, with resonator 3 loaded. The theoretical results in Table IV are used as reference. Resistors are paralleled so as to obtain practical values close to theoretical optimized ones. Capacitors are connected in series so that the practical values are close to theoretical optimized values. The practical test conditions are as follows:

1) identical resonators with both the load and operating frequency optimized, but operated at resonance frequency (f_o) of the resonators ($R_L = 16.94\ \Omega$; $f = f_0 = 520$ kHz);
2) identical resonators with both the load and operating frequency optimized, but operated at the optimized frequency ($R_L = 16.94\ \Omega$ (close to theoretical value of 17.04 Ω); $f = 0.9855 f_0 = 512$ kHz);
3) resonators with the load and the capacitor values optimized for the given frequency operation ($R_L = 11.23\ \Omega$ (close to theoretical value of 12.52 Ω); $C_2 = 0.9393 C_0$ (close to the theoretical $0.9448 C_0$); $f = 520$ kHz).

The current waveforms for the resonators are captured for evaluation. Fig. 16 shows the set of practical current waveforms for case (b). These waveforms are stored and then processed so that their vector diagrams can be produced. With $\mathbf{I_1}$ normalized as vector $\mathbf{1}$, Fig. 17(a)–(c) are the vector diagrams for the three test conditions test-(a), test-(b), and test-(c), respectively. The dotted vectors are the theoretical predictions and the solid vectors are practical measurements. It can be seen that the theoretical predictions of the relative magnitudes and phases of the current vectors in the resonators are generally consistent with practical measurements. The slight errors in the phase of some vectors are thought to be due to the tolerance of the capacitors and the inductances of the windings. Since $\mathbf{I_3}$ flows through the load in resonator 3, a high efficiency can be achieved if $\mathbf{I_2}$, which causes conduction loss in resonator 2, is small in magnitude. Comparison of the three vector diagrams shows that magnitude of $\mathbf{I_2}$ is the smallest in case (c) and the largest in case (a). This explains why the efficiency is highest in case (c) and lowest in case (a). The use of the vector diagrams therefore provides the physical insights in understanding the behavior of the circular domino-resonator systems. The measured and theoretical energy efficiencies of the three-resonator system with resonator 3 loaded under the three test conditions are shown in Fig. 18. These measurements confirm the validity and accuracy of the theoretical analysis. It is important to note that the control of the resonator impedance is an effective way for power flow control in wireless domino-resonator systems [23]. The results of case (c) in Fig. 18 indicate that high efficiency can be attained over a wider frequency range if the capacitor values can be controlled.

B. Circular Four-Resonator System

A circular four-resonator system has also been tested. Experiments are conducted to evaluate such system with resonators 2 and 3 loaded separately, under different sets of optimized variables.

1) With Resonator 2 Loaded: Experiments are firstly conducted on the systems with resonator 2 loaded under three

TABLE V
PERFORMANCE OF THE FOUR-RESONATOR SYSTEM WITH RESONATOR 2 LOADED UNDER DIFFERENT OPTIMIZATION METHODS

	C_2/C_0	C_3/C_0	C_4/C_0	f/f_0	R_L [Ω]	η
OPT(R_L)	1	1	1	1	5.85	3.76%
OPT(f, R_L)	1	1	1	0.9736	20.56	75.00%
OPT(C_2, C_3, C_4, R_L)	0.9924	0.9137	0.9137	1	11.57	83.01%

TABLE VI
PERFORMANCE OF THE FOUR-RESONATOR SYSTEM WITH RESONATOR 3 LOADED UNDER DIFFERENT OPTIMIZATION METHODS

	C_2/C_0	C_3/C_0	C_4/C_0	f/f_0	R_L [Ω]	η
OPT(R_L)	1	1	1	1	16.60	78.68%
OPT(f, R_L)	1	1	1	0.9885	18.07	80.68%
*OPT(C_2, C_3, C_4, R_L)	0.9712	0.9920	0.9712	1	16.56	81.73%

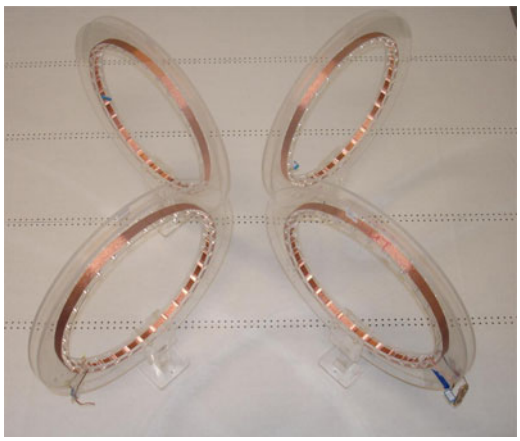

Fig. 15. Circular four-resonator system.

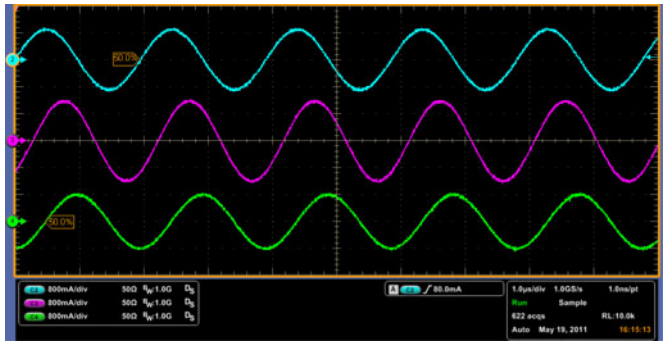

Fig. 16. Current waveforms of the circular three-resonator system with identical resonators operating at 512 kHz. [Case (b)]:$\mathbf{I_1}$: channel 2 (blue); $\mathbf{I_2}$: channel 3 (purple), and $\mathbf{I_3}$: channel 4 (green).

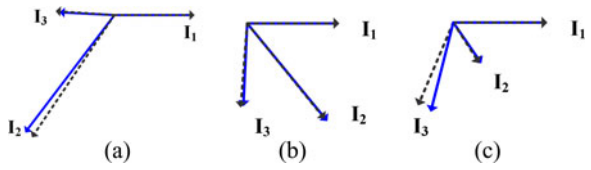

Fig. 17. Current vectors of the circular three-resonator systems with the current in resonator 1 as vector **1**. (a) Identical resonators: 520 kHz. (b) Identical resonators: 512 kHz. (c) C_2 adjusted: 520 kHz.

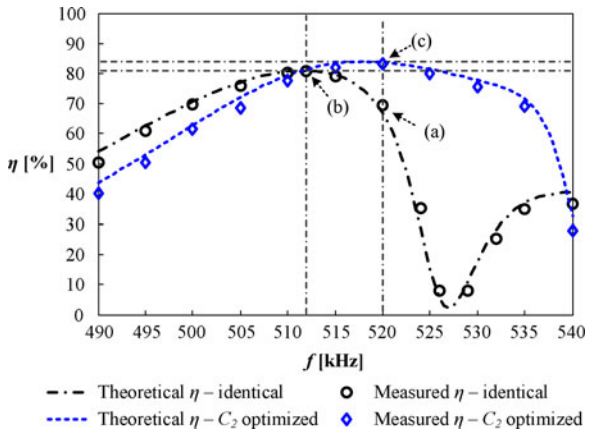

Fig. 18. Energy efficiency curves of the circular three-resonator systems under the test conditions (a), (b), and (c). (Note: "identical" represents the system with identical resonators and "C_2 optimized" represents the system with C_2 adjusted to a near optimum value.)

different sets of optimization criteria. The theoretical results in Table V are used as reference:

1) identical resonators with both the load and operating frequency optimized, but operated at resonance frequency (f_o) of the resonators ($R_L = 21.20\ \Omega$; $f = f_0 = 520$ kHz);
2) identical resonators with both the load and operating frequency optimized, but operated at the optimized frequency ($R_L = 21.20\ \Omega$ (close to theoretical value of 20.56 Ω); $f = 0.9736 f_0 = 505$ kHzo;
3) resonators with the load and the capacitor values optimized for the given frequency operation ($R_L = 11.82\ \Omega$ (close to theoretical value of 11.57 Ω); $C2 = 0.9130 C_0$ (close to the theoretical $0.9137 C_0$); $f = 520$ kHz).

The current vectors of the resonators under test condition (b) are shown in Fig. 19. The current vector diagrams are plotted in Fig. 20, with $\mathbf{I}_1$ normalized as vector 1. It should be noted that the relative magnitude of $\mathbf{I_2}$ is very small. Therefore, an "enlarged" $\mathbf{I}_2$ vector with 10 times the magnitude is shown in Fig. 20 for easy inspection. The solid vectors are measurements and the dotted ones are theoretical predictions. The measured and theoretical energy efficiency curves are shown in Fig. 21. Both the current vectors and the efficiency curves agree well with the theoretical predictions.

It is important to note in Fig. 21 that efficiency at (a) (resonant frequency, 520 kHz) is close to zero. It has been predicted in Fig. 10(b) that $\mathbf{I_{2\_P1}}$ and $\mathbf{I_{2\_P2}}$ are out of phase and therefore

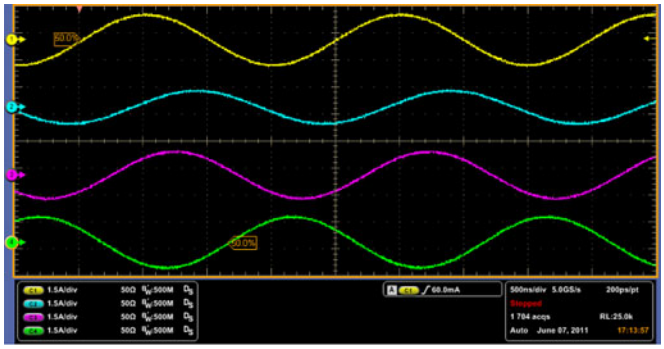

Fig. 19. Current waveforms of the circular four-resonator system with identical resonators, loaded at resonator 2 and operating at 505 kHz. $\mathbf{I_1}$ is displayed at channel 1 (yellow); $\mathbf{I_2}$ channel 2 (blue); $\mathbf{I_3}$ channel 3 (purple), and $\mathbf{I_4}$ channel 4 (green, 180° out of phase with the $\mathbf{I_4}$ shown in Fig. 20).

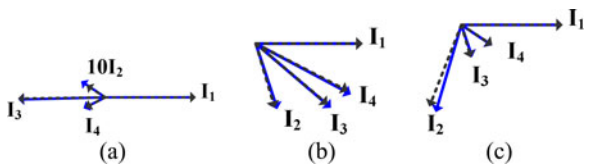

Fig. 20. Current vectors of the two circular four-resonator systems with the current in resonator 1 as vector 1. (a) Identical resonators: 520 kHz. (b) Identical resonators: 505 kHz. (c) C_3 and C_4 optimized: 520 kHz.

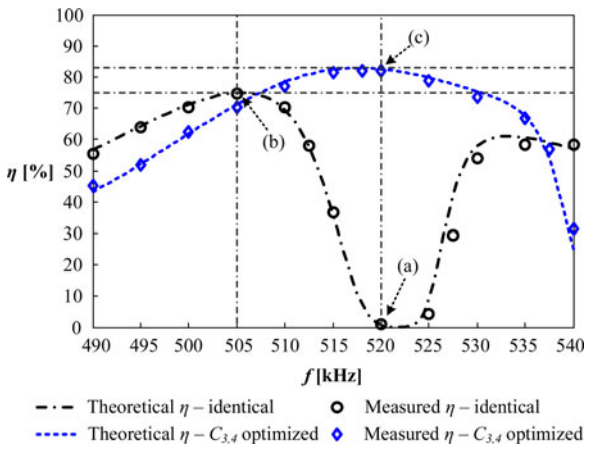

Fig. 21. Energy efficiency curves of the two circular four-resonator systems with resonator 2 loaded under the test conditions (a), (b), and (c).

counteract each other, resulting in a very low efficiency. The measured result confirms the validity of the theoretical analysis. By shifting the operating frequency from the resonant frequency to the optimized frequency, the vector diagram changes from that in Fig. 20(a) to that in Fig. 20(b). A much larger $\mathbf{I_2}$ is now generated to power the load. It can also be observed that optimizing the capacitors offers even higher energy efficiency. This can be understood from the corresponding vector diagram in Fig. 20(c). The magnitudes of $\mathbf{I_3}$ and $\mathbf{I_4}$ are smaller in Fig. 20(c) than in Fig. 20(b), implying that the conduction losses in resonators 3 and 4 are lower.

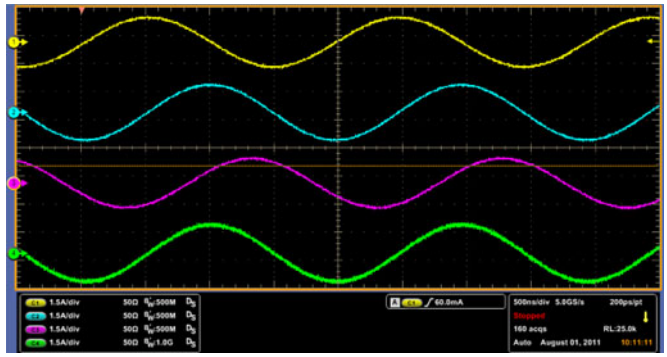

Fig. 22. Measured currents in the circular four-resonator system with resonator 3 loaded at 513 kHz.

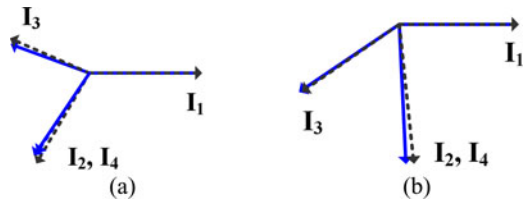

Fig. 23. Current vectors of the circular four-resonator system with the current in resonator 1 as vector 1. (a) Identical resonators: 520 kHz. (b) Identical resonators: 513 kHz.

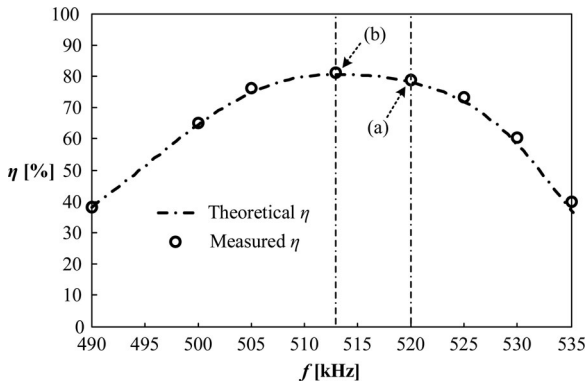

Fig. 24. Energy efficiency curve of the circular four-resonator system with resonator 3 loaded.

2) With Resonator 3 Loaded: Finally, the four-resonator system is tested with resonator 3 loaded. The theoretical results in Table VI are used as reference. Since the optimized capacitors in Table VI are all closed to C_0, only two test cases are considered here:

1) identical resonators with both the load and operating frequency optimized, but operated at resonance frequency (f_o) of the resonators ($R_L = 18.38\ \Omega$; $f = f_0 = 520$ kHz);
2) identical resonators with both the load and operating frequency optimized, but operated at the optimized frequency ($R_L = 18.38\ \Omega$ (close to theoretical value of 18.07 Ω); $f = 0.9885 f_0 = 513$ kHz).

The resonator currents are captured at the resonance frequency (520 kHz) and at optimized frequency (513 kHz). Fig. 22

shows the measured resonator currents in the four-resonator system with resonator 3 loaded under optimized frequency operation. The measured vector diagrams under these two operating frequencies are displayed in Fig. 23. The theoretical energy efficiency curve and the measured efficiencies are plotted in Fig. 24. These results generally have good agreements. Once again, when more than one pair of resonators are used in a domino manner, the multiple power path effects will cause the maximum efficiency point to shift away from the resonance frequency, as can be seen in Fig. 24.

V. Conclusion

In this paper, the mathematical formulation of wireless domino-resonator systems with noncoaxial resonators is presented. It is employed to analyze circular systems, which have two main power flow paths. The interactions of the two paths are analyzed with superposition principle and explained with the help of the vector diagrams. It is discovered that, under resonant frequency operation, current vector counteraction and reenforcement could occur in some resonators of the systems with even number of resonators. Such phenomenon does not occur in systems with odd number of resonators at resonant frequency. However, it is shown that the optimized operating frequency of wireless domino-resonator systems is not the resonant frequency of the resonators, as previously reported by Tesla for wireless power transfer via one pair of resonators. The reason is that the multiple power path effects of the resonator systems would shift the optimal frequency slightly away from the resonant frequency. The theoretical and practical investigations here have confirmed one important conclusion that optimized frequency operation can avoid current counteraction effects even in systems with even number of resonators. In addition, it has been successfully demonstrated that controlling the compensating capacitance could alter the impedance of the power flow paths and offer larger high-energy-efficiency frequency range for wireless domino-resonator systems.

References

[1] H. Winfield Secor, "Tesla apparatus and experiments—How to build both large and small Tesla and Oudin coils and how to carry on spectacular experiments with them," *Practical Electrics*, Nov. 1921.

[2] R. Lomas, The Man Who Invented the Twentieth Century: Nikola Tesla, Forgotten Genius Of electricity. London, U.K: Headline Book Publishing, 1999, p. 146.

[3] J. C. Schuder, H. E. Stephenson, Jr., and I. F. Townsend, "High-level electromagnetic energy transfer through a closed chest wall," in *IRE Int. Conf. Rec.,* Pt. 9, 1961, vol. 9, pp. 119–126.

[4] C. F. Andrea, M. A. Fadpli, V. L. Gott, and S. R. Topaz, "The skin tunnel transformer: A new system that permits both high efficiency transfer of power and telemetry of data through the intact skin," *IEEE Trans. Biomed. Eng.*, vol. 15, no. 4, pp. 278–280, Oct. 1968.

[5] J. C. Schuder, I. H. Gold, and H. E. Stephenson, Jr, "An inductively coupled RF system for the transmission of 1 kW of power through the skin," *IEEE Trans. Biomed. Eng*, vol. 18, no. 4, pp. 265–272, Jul. 1971.

[6] A. Ghahary and B. H. Cho, "Design of a transcutaneous energy transmission systems using a series resonant converter," in *Proc. IEEE Power Electron. Spec. Conf.*, Jun. 1990, pp. 1–8.

[7] G. B. Joung and B. H. Cho, "An energy transmission system for an artificial heart using leakage inductance compensation of transcutaneous transformer," *IEEE Trans. Power Electron.*, vol. 13, no. 6, pp. 1013–1022, 1988.

[8] H. H. Wu, J. T. Boys, and G. A. Covic, "An AC processing pickup for IPT systems," *IEEE Trans. Power Electron.*, vol. 25, no. 5, pp. 1275–1284, May 2010.

[9] G. A. Covic, J. T. Boys, M. L. G. Kissin, and H. G. Lu, "A three-phase inductive power transfer system for roadway-powered vehicles," *IEEE Trans. Ind. Electron.*, vol. 54, no. 6, pp. 3370–3378, Dec. 2007.

[10] H. H. Wu, G. A. Covic, J. T. Boys, and D. J. Robertson, "A series-tuned inductive-power-transfer pickup with a controllable AC-voltage output," *IEEE Trans. Power Electron.*, vol. 26, no. 1, pp. 98–109, Jan. 2011.

[11] Y. Jang and M. M. Jovanovic, "A contactless electrical energy transmission system for portable-telephone battery chargers," *IEEE Trans. Ind. Electron.*, vol. 50, no. 3, pp. 520–527, Jun. 2003.

[12] C.-G. Kim, D.-H. Seo, J.-S. You, J.-H. Park, and B. H. Cho, "Design of a contactless battery charger for cellular phone," *IEEE Trans. Ind. Electron.*, vol. 48, no. 6, pp. 1238–1247, Dec. 2001.

[13] S. Y. R. Hui and W. C. Ho, "A new generation of universal contactless battery charging platform for portable consumer electronic equipment," *IEEE Trans. Power Electron.*, vol. 20, no. 3, pp. 620–627, May 2005.

[14] X. Liu and S. Y. R. Hui, "Simulation study and experimental verification of a contactless battery charging platform with localized charging features," *IEEE Trans. Power Electron.*, vol. 22, no. 6, pp. 2202–2210, Nov. 2007.

[15] S. Y. R. Hui, "Planar inductive battery charging system," U.S. Patent 7 576 514, 2009.

[16] B. Choi, J. Nho, H. Cha, T. Ahn, and S. Choi, "Design and implementation of low-profile contactless battery charger using planar printed circuit board windings as energy transfer device," *IEEE Trans. Ind. Electron.*, vol. 51, no. 1, pp. 140–147, Feb. 2004.

[17] Wireless Power Consortium Website. [Online]. Available: http://www.wirelesspowerconsortium.com/

[18] M. A. Keyes and R. L. Yeager, "Wireless power transmission systems and methods,", U.S. Patent US 2007/0021140A1, Jan. 25, 2007.

[19] E. Waffenschmidt and T. Staring, "Limitation of inductive power transfer for consumer applications," in *Proc. Eur. Conf. Power Electron. Appl.*, 2009, pp. 1–10.

[20] Jośe Oscar Mur-Miranda *et al.*, "Wireless power transfer using weakly coupled magnetostatic resonators," *IEEE ECCE Conf.*, 2010, pp. 4179–4186,.

[21] F. Zhang, S. Hackworth, W. Fu, and M. Sun, "The relay effect on wireless power transfer using witricity," in *Proc. IEEE Conf. Electromagn. Field Comput.*, May 9–12, 2010, Chicago, II.

[22] R. Syms, E. Shamonina, and L. Solymar, "Magneto-inductive waveguide devices," *IEE Proc. Microw., Antennas Propag.*, vol. 153, no. 2, pp. 111–121, Apr. 2006.

[23] C. K. Lee, W. X. Zhong, and S. Y. R. Hui, "Effects of magnetic coupling of nonadjacent resonators on wireless domino-resonator systems," *IEEE Trans. Power Electron.*, vol. 27, no. 4, pp. 1905–1916, 2012.

[24] J. C. Maxwell, *A Treatise on Electricity and Magnetism*. New York: Dover, 1954 (reprint from the original from 1873).

[25] F. W. Grover, *Inductance Calculations*. New York: Dover, 1964.

[26] S. I. Babic and C. Akyel, "Calculating mutual inductance between circular coils with inclined axes in air," *IEEE Trans. Magn.*, vol. 44, no. 7, pp. 1743–1750, Jul. 2008.

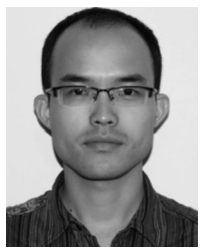

W. X. Zhong was born in China, in 1984. He received the B.S. degree in electrical engineering from Tsinghua University, Beijing, China, in 2007. He is currently working toward the Ph.D. degree at the Center for Power Electronics, City University of Hong Kong, Kowloon, Hong Kong.

His current research interests include synchronous rectification and wireless power transfer.

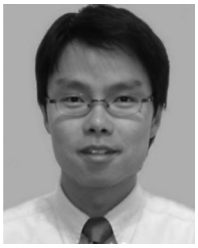

Chi Kwan Lee (M'04) received the B.Eng. and Ph.D. degrees in electronic engineering from the City University of Hong Kong, Kowloon, Hong Kong, in 1999 and 2004, respectively.

From 2004 to 2005, he was a Postdoctoral Research Fellow at the Power and Energy Research Centre, National University of Ireland, Galway, Ireland. In 2006, he became a Research Fellow at the Centre of Power Electronics, City University of Hong Kong. In 2008–2011, he was a Lecturer of Electrical Engineering at the Hong Kong Polytechnic University. Presently, he is an Assistant Professor at the Department of Electrical & Electronic Engineering, University of Hong Kong. His current research interests include applications of power electronics to power systems, advanced inverters for renewable energy and smart grid applications, reactive power control for load management in renewable energy systems, wireless power transfer, energy harvesting, and planar electromagnetics for HF power converters.

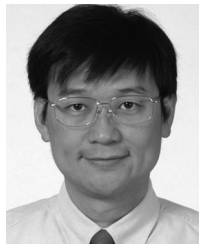

S. Y. (Ron) Hui (F'03) received the Ph.D. degree from Imperial College London, London, U.K., in 1987.

He has previously held academic positions at the University of Nottingham, the University of Sydney, and City University of Hong Kong. In 2011, he joined the University of Hong Kong as Chair Professor. Concurrently, since 2010, he has held the Chair Professorship of Power Electronics at Imperial College London. He has published over 200 technical papers, including more than 160 refereed journal publications and book chapters. Over 50 of his patents have been adopted by industry.

Dr. Hui is a Fellow of the Institution of Engineering and Technology (IET). He has been an Associate Editor of the IEEE TRANSACTIONS ON POWER ELECTRONICS since 1997 and an Associate Editor of the IEEE TRANSACTIONS ON INDUSTRIAL ELECTRONICS since 2007. He has been appointed twice as an IEEE Distinguished Lecturer by the IEEE Power Electronics Society in 2004 and 2006. He served as one of the 18 Administrative Committee members of the IEEE Power Electronics Society and was the Chairman of its Constitution and Bylaws Committee from 2002 to 2010. He received the Excellent Teaching Award at CityU in 1998 and the Earth Champion Award in 2008. He won an IEEE Best Paper Award from the IEEE IAS Committee on Production and Applications of Light in 2002, and two IEEE Power Electronics Transactions Prize Paper Awards for his publications on Wireless Battery Charging Platform Technology in 2009 and on LED system theory in 2010. His inventions on wireless charging platform technology underpin key dimensions of "Qi," the world's first wireless power standard, with freedom of positioning and localized charging features for wireless charging of consumer electronics. In November 2010, he received the IEEE Rudolf Chope R&D Award from the IEEE Industrial Electronics Society, the IET Achievement Medal (The Crompton Medal), and was elected to the Fellowship of the Australian Academy of Technological Sciences and Engineering.